Oligomeric odd-even effect in liquid crystals

SCHOLARONE™
Manuscripts

Conceptual insights statement

Odd-even effects, oscillations in properties of materials comprised of an odd or even number of connected repeating units, are well-known phenomena in materials science. In organic materials, they are usually associated with the number of methyl groups in aliphatic chains. In this work, we unveil multiple signatures of a new odd-even effect in liquid crystals that occurs at the larger scale of molecular moieties that by themselves express liquid crystalline behavior. Namely we show that oligomeric liquid crystals, with n=1-4 number of rigid mesogenic segments connected by flexible aliphatic chains with an odd number of methyl groups, produce an odd-even effect in optical anisotropy and the bend elastic constant of the liquid crystal oligomer. We also demonstrate that even in the absence of long-range electron density modulation, careful analysis of synchrotron SAXS results can provide important information about the molecular associations both in the N and NTB phases. This novel odd-even effect opens up a new mode to optimize phase and optical behavior.

Oligomeric odd-even effect in liquid crystals

Rony Saha[1], Greta Babakhanova[2, 3], Zeinab Parsouzi[1], Mojtaba Rajabi[1], Prabesh Gyawali[1],

Chris Welch[4], Georg H. Mehl[4,†], James Gleeson[1], Oleg D. Lavrentovich[1,2, 3,†], Samuel Sprunt[1,*],

and Antal Jákli[1, 2, 3, *]

[1]Physics Department, Kent State University, Kent, OH 44242, USA
[2]Advanced Materials and Liquid Crystal Institute, Kent State University, Kent, OH 44242, USA
[3]Chemical Physics Interdisciplinary Program, Kent State University, Kent, OH 44242, USA
[4]Department of Chemistry, University of Hull, Hull, UK

*Corresponding authors: ajakli@kent.edu, ssprunt@kent.edu
†olavrent@kent.edu, g.h.mehl@hull.ac.uk

Abstract:

Odd-even effects, oscillations in properties of materials comprised of an odd or even number of connected repeating units, are well-known phenomena in materials science. In organic materials, they are usually associated with the number of methylene groups in aliphatic chains. In this work, we unveil multiple signatures of a new odd-even effect in liquid crystals that occurs at the larger scale of molecular moieties that by themselves express liquid crystalline behavior. We demonstrate that oligomeric liquid crystals, with n=1-4 number of rigid mesogenic segments connected by flexible aliphatic chains with an odd number of methylene groups, produce an odd-even effect in optical anisotropy and the bend elastic constant of the liquid crystal oligomer. This effect is different from the usual odd-even effects with respect to the parity of carbon atoms in an aliphatic chain and can be understood in term of the average molecular shape and the associations between n-mers based on the packing of these shapes. We also show that, in spite of the fact that there is no long-range electron density modulation, careful analysis of synchrotron SAXS results can provide important information about the molecular associations in the N and N_{TB} phases that other techniques cannot access. This novel odd-even effect opens up a new mode to optimize phase and optical behavior.

Introduction

Odd-even effects are well-known in chemistry since Baeyer noticed that the melting points of fatty acids do not show a monotonic increase with increasing chain length and that the melting points of the members with even numbers of C atoms are higher than those of the members with odd numbers.[1] Similar melting point alternations are also known for short-chain n-alkanes.[2]

Similar odd-even effects were first described in liquid crystal dimers in 1927.[3] The nematic-to-isotropic transition temperature was observed to alternate with the parity of the number k of carbon atoms in the flexible link connecting two rigid rod-like cores[4,5]. The most obvious factor that explains this odd-even effects is the difference in the shapes of molecules. Since two neighboring methylene groups along the $(CH_2)_k$ linkage prefer to maximally separate their hydrogen pairs from each other, the H atoms of one group are above the C-C bond, while the H atoms of the neighboring groups are below the bond, forming a "trans" conformation. In such a conformation, the rigid cores connecting the end segments of the $(CH_2)_k$ linker are roughly parallel to each other when k is an even number and make approximately a 120° angle with each other when k is an odd number.

The same reasoning is used to explain the odd-even effects for semi-flexible main chain liquid crystal polymers[6–8]. Interestingly, for main-chain liquid crystalline polyethers, in which semi-rigid units are connected by flexible spacers with $k = 5, 7, 9$, an additional nematic ("N_x") phase appeared below the usual uniaxial N phase, while no "secondary" nematic was detected in the homologs with an even k.[9] In a homologous series of dimeric cyanobiphenyls, 1,7-bis(4,4'-cyanobiphenyloxy)alkanes *(CBkCB)*, with $k = 1 − 12$, in addition to an odd-even alternation of the I-N phase transitions [10], the transition entropies were found to be much higher for even k than for odd k, showing that the even dimers are significantly better ordered in the nematic phase than their odd counterparts [11]. Additionally, the formation of smectic-type focal-conic textures was observed below the N phase in odd k homologs. Based on polarized optical microscopy (POM) observations, the low temperature state was proposed to be a smectic phase. However, later x-ray diffraction studies found no evidence of an electron density modulation, showing that the lower temperature phase is a new type of nematic (N_X) phase rather than a smectic phase.[9,12–14] The discrepancy between the x-ray and POM observations led to an intense research that eventually concluded that the N_X phase is a twist-bend nematic (N_{TB}) phase, one of the most intriguing,

manifestations of molecular orientational order discovered in soft matter[12,14–23]. Freeze-fracture transmission electron microscopy (FFTEM) [16,24], solid state NMR studies[11,25] and resonant soft X-ray scattering (RSoXS) [26] studies later confirmed the modulated orientational order and showed that the pitch (modulation period) is remarkably short, p_{TB}~10 nm, two orders of magnitude smaller than in typical chiral nematic (cholesteric) materials.

In addition to liquid crystal dimers with odd ($k=5,7,9,11,13$) $(CH_2)_k$ linkages, higher oligomers (n-mers with $n>2$ mesogenic units) and odd parity flexible linkages between the mesogenic units[27–30] also exhibit the N_{TB} phase. In particular, carbon-edge RSoXS and FFTEM measurements[31] indicated that the nanoscale pitch p_{TB} of a trimer is almost temperature independent and is considerably shorter (6.6-6.7 nm) than that of the homologous dimer (10-18 nm), indicating that the nanoscale pitch and physical properties of the N_{TB} phase depend significantly on n.

Recently we presented a comparative study of the orientational (Frank) elastic constants and associated orientational viscosities in the uniaxial N phase of the dimer 5-Bis(2′,3′-difluoro-4,4″-dipentyl-[1,1′:4′,1″-terphenyl]-4-yl)nonane (DTC5-C9), and its homologous trimer (DTC5-C9-DTC-C9-DTC5) and tetramer (DTC5-C9-DTC-C9-DTC-C9-DTC5) (see Figures 2a-4a), all of which contain the same odd parity methylene linkage between the mesogenic units and exhibit a N-N_{TB} transition[32]. The temperature dependences of these parameters showed differences in the pretransitional behavior of some of the measured parameters, especially in the bend elastic constant K_{33}. After decreasing, on cooling, through most of the uniaxial N phase, K_{33} abruptly starts increasing in the dimer and tetramer close to the transition; while there is no indication of an increase in the trimer. Such behavior was found to be in qualitative agreement with the predictions of a coarse-grained theory, which models the N_{TB} phase as a "pseudo-layered" structure with the symmetry (but not the mass density wave) of a smectic-A phase.

In this paper we show the presence of novel, so far not reported odd-even effect in oligomers with respect to the number (n=1-4) of the mesogenic units connected by $(CH_2)_k$ linkages (see Figure 1). Temperature dependent birefringence and small-angle x-ray scattering (SAXS) measurements on monomer MCT5 (2′, 3′-difluoro-4,4″-dipentyl-p-terphenyl)[33], its dimer (DTC5-C9), trimer (DTC5-C9-DTC-C9-DTC5)   and tetramer (DTC5-C9-DTC-C9-DTC-C9-DTC5) homologs[32] show that the liquid crystal phase ranges, the optical birefringence (refractive index anisotropy), characteristic wavenumber of the short-range, spatial variations of the electron

density, and the bend elastic constant show an odd-even effect with respect to the number of monomer units, n. We describe how this effect can be understood in term of the average molecular shape of the n-mers and their intermolecular associations. We also show that, though there is no long-range electron density modulation, careful analysis of synchrotron SAXS results can provide important information about the structure both in the N and N_{TB} ranges that other techniques cannot so readily or conveniently access.
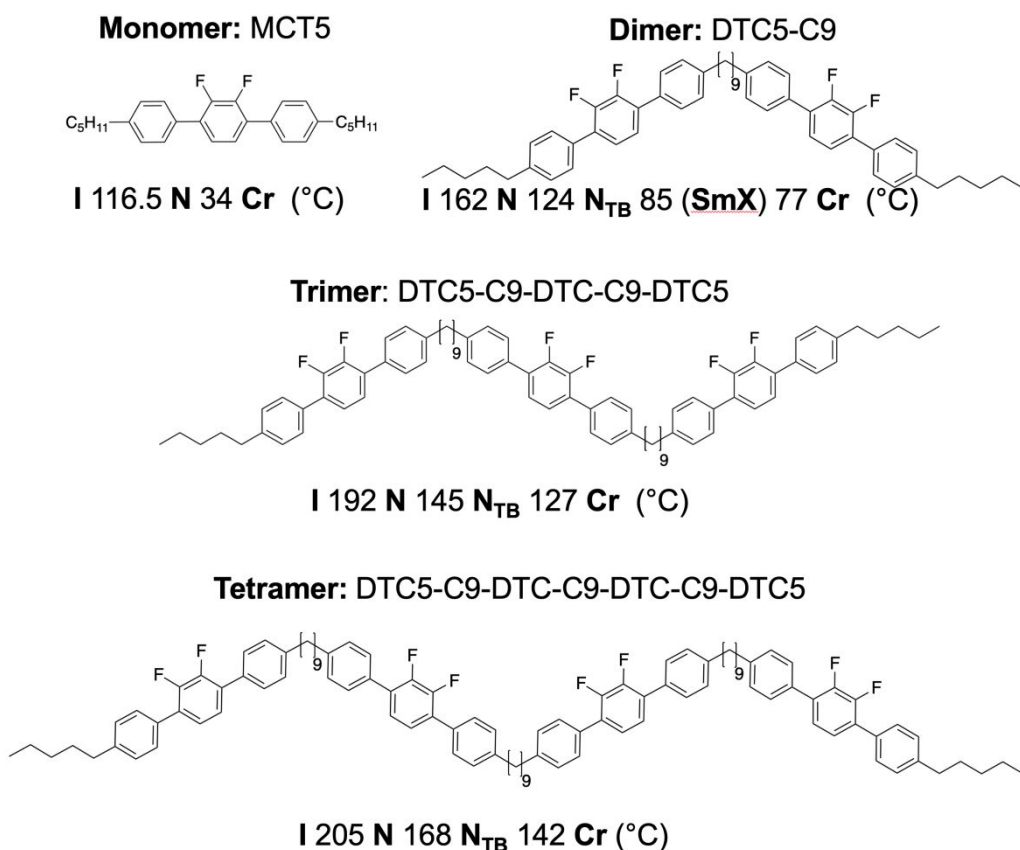
Monomer: MCT5

Dimer: DTC5-C9

I 116.5 **N** 34 **Cr** (°C)   I 162 **N** 124 N_{TB} 85 (**SmX**) 77 **Cr** (°C)

Trimer: DTC5-C9-DTC-C9-DTC5

I 192 **N** 145 N_{TB} 127 **Cr** (°C)

Tetramer: DTC5-C9-DTC-C9-DTC-C9-DTC5

I 205 **N** 168 N_{TB} 142 **Cr** (°C)

Figure 1: Molecular structures and phase transition temperatures of the studied n=1-4 oligomers.

Experimental Methods

Optical birefringence studies were performed in cells treated for homogeneous planar alignment of the nematic director. Prior to filling each cell, using a UV/VIS Spectrometer (Perkin Elmer, Lambda 18), we determined the gap between the substrates to an accuracy of a few percent or less. The sample thicknesses ranged from 3.6 to 5.1 μm. For temperature-dependent measurements, the sample cells were placed in an Instec HCS402 hot stage (regulated to a precision of 0.01˚C). To determine the optical birefringence $\Delta n = n_e - n_o$ (where n_o and n_e are the ordinary and extraordinary refractive indices), we measured the phase shift $\Delta\phi$ of polarized green

4

light (λ = 546 nm) transmitted through homogeneously aligned samples of uniform thickness d, using both an optical Abrio LC-PolScope and a Berek U-CTB phase compensator (Olympus). The birefringence Δn is given by $\Delta n = \lambda \Delta \phi / 2 \pi d$.

Small angle x-ray scattering (SAXS) measurements were carried out on the CMS beamline 11-BM at NSLS II in Brookhaven National Laboratory with the x-ray energy set at 17 keV. Samples of dimer, trimer, and tetramer were loaded into the bottom 5 mm of 1 mm diameter quartz capillaries with 10 μm wall thickness. The capillaries were inserted into a temperature regulated hot stage, which could be reproducibly positioned in the X-ray beam. The sample-containing volume was located between narrowly spaced samarium cobalt magnets, which applied a uniform 1.2 Tesla field across the sample and perpendicular to the incident beam, in order to align the nematic director. Homogeneous alignment was achieved by first heating the samples into the isotropic phase and then slowly (rate: 1°C/min) cooling into the uniaxial nematic. Two-dimensional SAXS patterns were recorded on an area detector (Dectris, Pilatus 2M) for various temperatures on both sides of the N–N$_{TB}$ transition.

Results and Discussion

Figure 2 (a) shows the normalized temperature dependence of the birefringence Δn for n=1-4-mers. The normalized temperature T' is defined as $T'= (T-T_{NTB})/(T_{NI}-T_{NTB})$ for n=2-4 and $T'=(T-T_{Cr})/(T_{NI}-T_{Cr})$ for n=1. Here T is the sample temperature and T_{NI}, T_{NTB}, T_{Cr} are the nematic-isotropic, nematic-twist bend nematic and crystallization temperatures, respectively. The birefringence of all four compounds is positive through the nematic range. The homologues with an odd number of core units (monomer and trimer) have higher birefringence than the consecutive even n-mers being the birefringence of the monomer the highest and of the dimer is the smallest. In comparison with DTC5-C7 (the same mesogenic units, but shorter methylene linkage), we find that $\Delta n(DTC5-C9)$ is slightly larger than $\Delta n(DTC5-C7)$[34] indicating increased aspect ratio of the molecules with longer linking group. From NMR measurements by Emsley et al. (see Figure 8 of [35]) on DTC5-C9 we find that the ratio of the nematic order parameters of the monomer and dimer measured at the same reduced temperature $T^*=(T_{NI}-T)/T_{NI}$ is very similar to the ratio of the birefringences. Since the birefringence Δn is proportional to the order parameter S [36], we conclude that the smaller birefringence of the dimer compared the monomer is due to the smaller order parameter. The temperature dependence of the birefringence of the dimer also shows a slight

pretransitional decrease in Δn as $T \rightarrow T_{NTB}$. Similar pretransitional decrease of the order parameter was seen by Emsley et al[35] indicating that the pretransitional decrease of Δn can also be attributed to the order parameter. The temperature behavior of the order parameter in the DTC5C9 dimer was explained in terms of the molecular bend angle and the pretransitional heliconical tilt θ that increases to about $\theta \sim 15^o$ as N_{TB} approached on cooling (Figure 11 of [35]). The pretransitional behavior of Δn is not obviously visible for the trimer and tetramer (see inset to Figure 2(a)), indicating that conformational changes have a weaker effect on the molecular anisotropy, are less temperature-dependent, or simply play a lesser role in the pretransitional behavior.
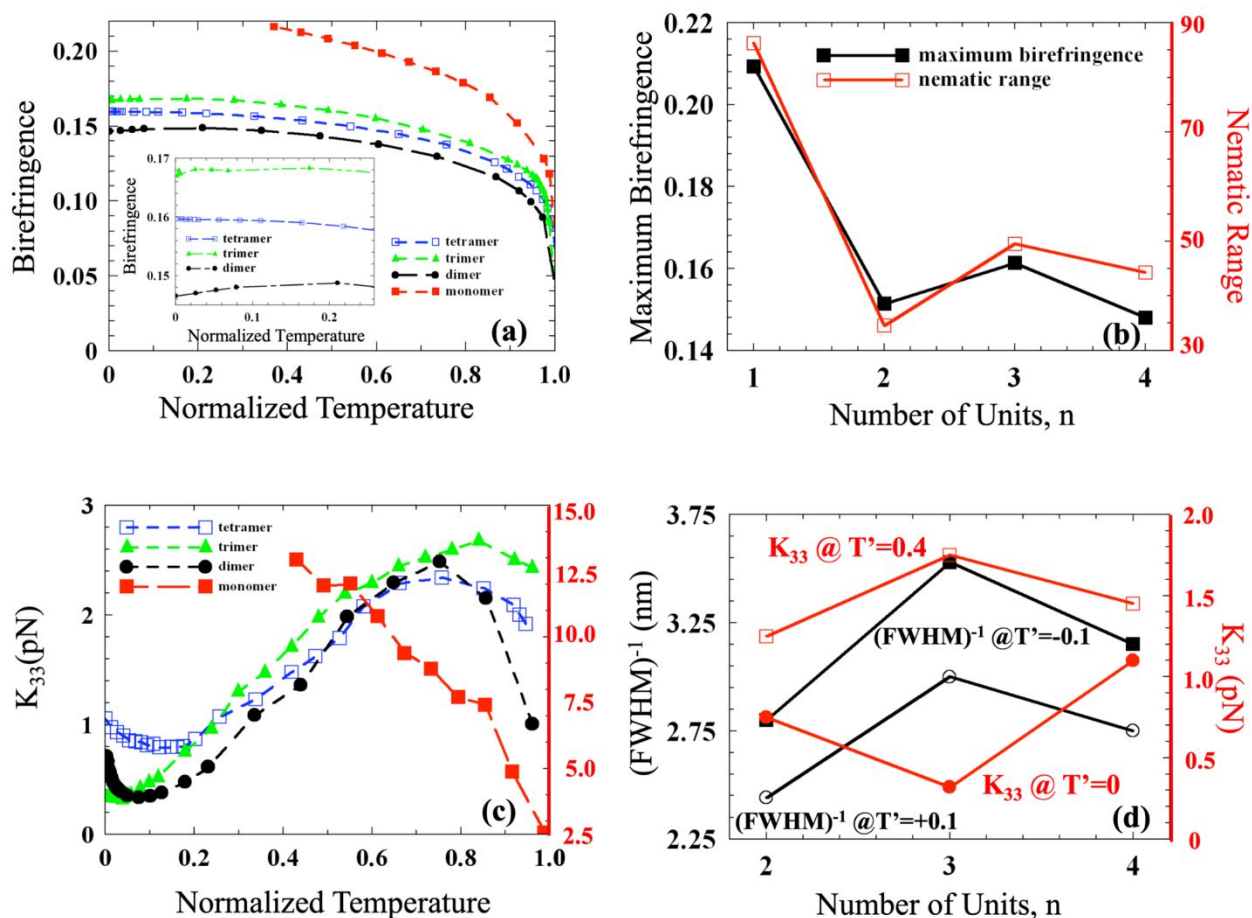

Figure 2: Demonstration of the odd-even effects in the studied n-mers. (a) Optical birefringence (Δn) as a function of normalized temperature (T') in the N phase of monomer, dimer, trimer, and tetramer (n=1-4). The normalized temperature is defined as T'= (T-T_{NTB})/(T_{NI}-T_{NTB}) for n=2-4 and T'=(T-T_{Cr})/(T_{NI}-T_{Cr}) for n=1, where T is the sample temperature and T_{NI}, T_{NTB}, T_{Cr} are the nematic-isotropic, nematic-twist bend nematic and crystallization temperatures respectively. (b) The maximum birefringence (left axis) and nematic ranges (right axis) as a function of the number of monomeric units n=1-4. (c) Normalized temperature dependences of the bend elastic constant K_{33}

of n=1-4 n-mers (for n=2-4 data is taken from [32]). d) Inverse full width at half maxima (FWHM)$^{-1}$ (left axis) and elastic constant K_{33} (right axis) for n=2-4 of n-mers at selected normalized temperatures.

In Figure 2(b) the maximum birefringence (left axis) and the nematic temperature range (right axis) are compared for n=1-4 n-mers. Both the maximum birefringence and the nematic temperature range are larger for odd n-mers. This can be understood by considering the shape of the n-mers. The monomer (n=1) is rod shaped with the highest aspect ratio, the trimer (n=3) has two units parallel and one at an angle, so its effective aspect ratio is larger compared to the dimer and tetramer (n=2,4), where successive monomeric units make an angle of about 120° with each other, producing shapes which can be simplified as twisted "V" and "W", respectively. We also observe that the N_{TB} range of the trimer (22°C) is lower than that of the dimer and tetramer (31°C and 25°C, respectively). The bent-shape therefore clearly destabilizes the N and stabilizes the N_{TB} phase. This is also related to the aspect ratio ε of the molecules: the higher is ε, the wider is the nematic phase. [11]

Results for the bend elastic constant (K_{33}) in the N phase of the n=1-4 n-mers[32] are displayed in Figure 2(c). We see odd-even effects in the K_{33} values far from the N-N_{TB} transition (*T' > 0.3*) and at the transition (*T' = 0*). In the vicinity of *T'~ 0.2*, the odd-even effect diminishes and changes sign: For *T' > 0.3* the bend elastic constant is larger in the trimer than in the even n-mers, but near the N-TB transition (*T' < 0.1*) this relation is clearly reversed. In the range *0 <T'< 0.2*, K_{33} for the dimer and tetramer starts to increase, while there is no such indication of a pretransitional enhancement for the trimer. For comparison, values of K_{33} among the n-mers at *T' = 0.4* and *0* are plotted against the right axis of Figure 2(d). The observed odd-even effect of the bend elastic constant K_{33} away from the transition may again be related to the overall shape of the n-mers. The effect of the molecular shape on K_{33} for nematic liquid crystals was first studied theoretically by Gruler [37] and Helfrich [38]. Helfrich argued that for bent-shaped molecules the strain of the bend distortion can be partly relieved by a rotation around the long axis of the individual molecules, thereby allowing more molecules to match their bent conformation to the externally imposed bend. Experimentally several groups found that K_{33} is indeed significantly smaller than K_{11} for bent-core materials [23,39–42]. Theoretical and experimental aspects of the effect of the molecular shape on K_{33} are discussed in detail in Reference[15]. As we argued above, the overall

shape of the trimer molecules is more linear than of dimer and tetramer, thus explaining the larger K_{33} of trimer relative to the dimer and tetramer away from the N-N_{TB} transition.

The inverse of the Full Width at Half Maxima (FWHM) of the diffuse peak, detected in our SAXS measurements at a wavenumber q corresponding to the monomer length represents the spatial extent of monomer-monomer correlations (correlation length) along the average long axis of the n-mers. It also reveals an odd-even effect, with the correlation length being larger for the trimer than for the dimer or tetramer. Examples at $T'=\pm0.1$ are plotted against the left axis of Figure 2(d). To understand this effect, and the pretransitional behavior of K_{33} shown in Figure 2c, we turn to our SAXS results (see Figures 3-5).
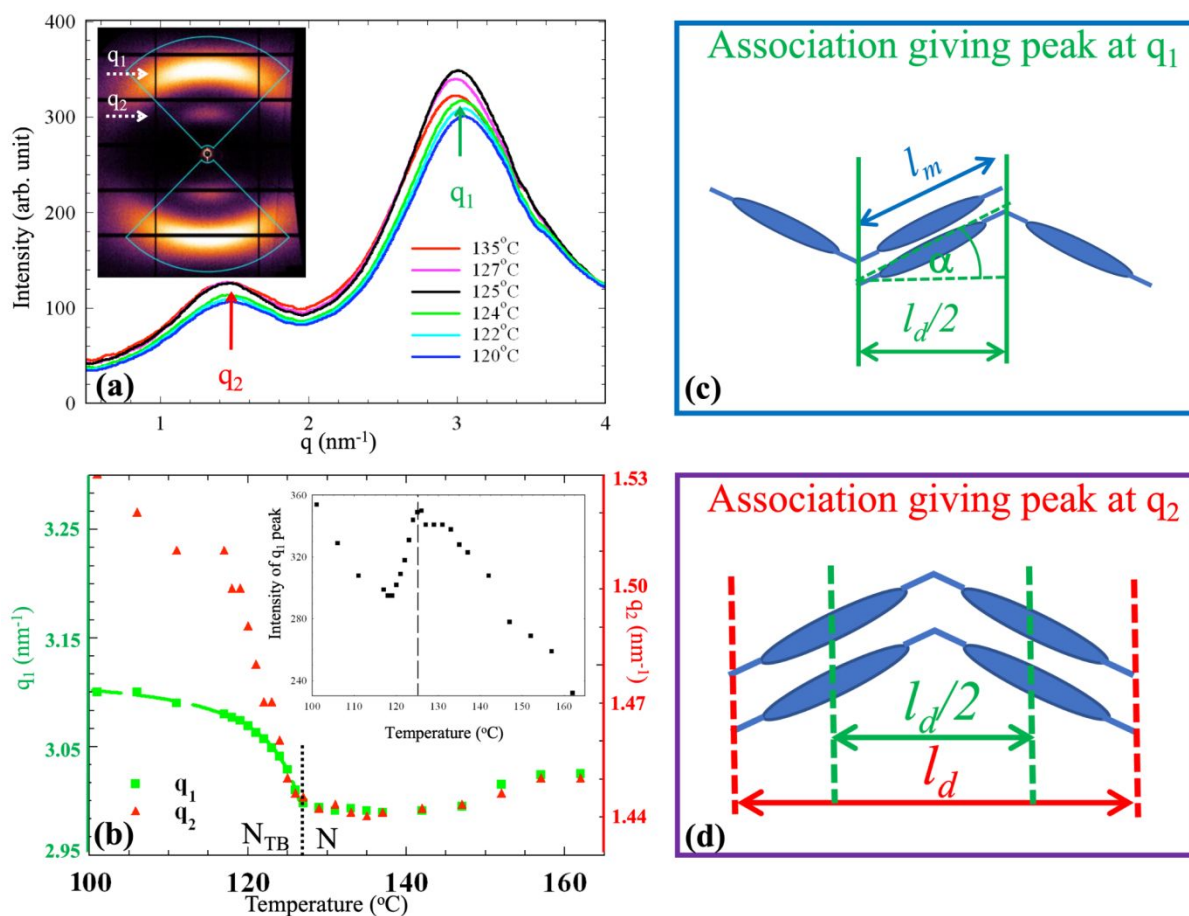

Figure 3: Summary of the Small Angle X-ray Scattering (SAXS) results and proposed molecular association models for the dimer. (a) Wavenumber (q) dependence of the scattered intensity for $0.5<q<4$ nm^{-1} at selected temperatures in the N and N_{TB} phases. Inset shows the 2D SAXS pattern in the nematic phase at 2°C above the N-N_{TB} phase transition. Dark lines represent gaps in the detector array. Sectors drawn with blue lines indicate the areas over which the intensity (I) was azimuthally averaged in order to produce the plots of I vs q (nm^{-1}) shown in the main pane. Maxima of the peaks are denoted by q_1 and q_2. (b)Temperature dependences of q_1 and q_2 are plotted on the left and right axes, respectively. Temperature dependence of the intensity at q_1 is shown in

the inset. (c) Schematic model of the molecular association corresponding to the peak at q_1. (d) Schematic model of the molecular association corresponding to the peak at q_2. The subscripts m, d and t on l stand for monomer, dimer and trimer, respectively.

Figures 3(a) – 5(a) show the wavenumber (q) dependence of the SAXS intensity in the range 0.5 nm^{-1}<q<4 nm^{-1} at selected temperatures in the N and N$_{TB}$ phases. The insets to Figures 3(a) – 5(a) show the 2D small-angle diffraction patterns in the nematic phase 2°C above the N-N$_{TB}$ phase transition. Sectors drawn with blue lines indicate the areas over which the intensity (I) was azimuthally averaged in order to produce the plots of I vs q (nm^{-1}) shown in the main pane. SAXS results on the dimer show two broad peaks at $q_1 \sim 3 \ nm^{-1}$ and $q_2 \sim 1.5 \ nm^{-1}$. They correspond to periodicities of $d_1 \sim 2.1$ nm and $d_2 = 4.2$ nm, respectively. Calculations by *ChemOffice* based on the symmetric molecular shape shown in Figure 1, confirm that d_2 is basically equal to the length of the dimer l_d. Therefore $d_1 \sim l_d/2$. Thus, the peak at q_1, which is ~3 times more intense than the peak at q_2, corresponds to the average spacing between monomer units along the bent-conformation of an n-mer. The molecular associations corresponding to q_1 and q_2 are illustrated in Figure 3(c,d). Note that we model the dimer molecules as two rigid rods connected at one point. Such a structure can always be placed on a plane, so we could choose the plane of drawing to be parallel to the molecular plane.

The I vs q data for the trimer and tetramer show three diffuse peaks (see Figure 4(a) and Figure 5(a), respectively. The main peak is centered on $q_1 \sim 3.1$-$3.2 \ nm^{-1}$, slightly larger q values than for the dimer. The q_2 and q_3 peaks are very weak, probably because the trimer and tetramer are much more flexible than of the dimer, thus disfavoring the larger than monomer-type associations. The ratios of the peak positions are $q_1/q_2 \sim 1.6$ and $q_1/q_3 \sim 3$ for the trimer and $q_1/q_2 \sim 2$ and $q_1/q_3 \sim 4$ for the tetramer. Our proposed models for the corresponding molecular associations are shown in Figures 4(c,d,e) and Figure 5(c,d,e) for the trimer and tetramer, respectively. Since only two rigid rods connected at one point can be placed on a plane, the trimer and the tetramer molecules may not fit on a plane. For the trimer we chose the plane of the drawing to be parallel to the dimer segment that is not associated to a monomer segment of another molecule. This way the periodicity of the q_1-type association is $l_m \cos\alpha$ (see Figure 4(c)), where α is the angle between the monomer and the line connecting the neighboring layers (green planes) of the association. The q_1 and q_2 type of associations now will make an angle β (see Figure 4(d))

with each other, thus making the length of the dimeric association equal to $2l_m \cos\alpha \cdot \cos\beta$. Since $q_1/q_2{\sim}1.6$ from our data, we have, $q_1/q_2 = 2l_m \cos\alpha \cdot \cos\beta / (l_m \cos\alpha) = 2\cos\beta \square 1.6$. This gives $\beta \square 36^o$. As illustrated in Figure 4(e), the length of the trimeric-type association is $3l_m \cos\alpha \cdot \cos\gamma$, where the geometric relation between γ and β is $\tan(\beta-\gamma) = 2\sin\beta / (2\cos\beta + 1)$, which gives $\gamma \square 12^o$. Therefore $q_1/q_3 = 3\cos\gamma = 2.93$ in reasonably good agreement with the observed $q_1/q_3{\sim}3$ ratio. These considerations therefore show that the trimer molecule is twisted and bent with respect to the plane of the dimeric unit.
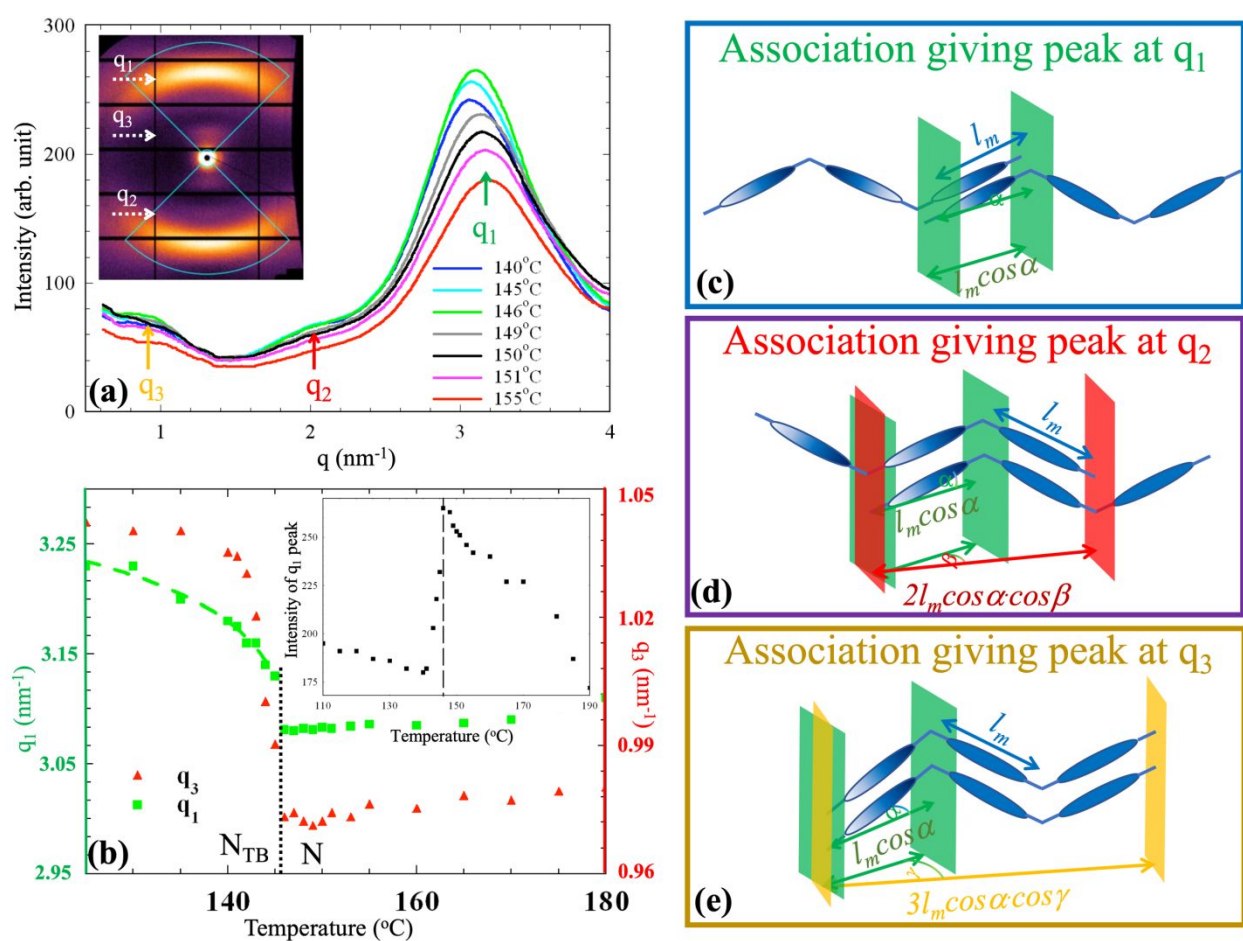

Figure 4: Summary of the SAXS results and proposed molecular association models for the trimer. (a) Wavenumber (q) dependence of the scattered intensity for $0.5<q<4$ nm^{-1} at selected temperatures in the N and N_{TB} phases. Inset shows the 2D SAXS pattern in the nematic phase at 2^oC above the N-N_{TB} phase transition. Dark lines represent gaps in the detector array. Sectors drawn with blue lines indicate the areas over which the intensity (I) was azimuthally averaged in order to produce the plots of I vs q (nm^{-1}) shown in the main pane. Maxima of the peaks are denoted by q_1, q_2 and q_3. (b)Temperature dependences of q_1 and q_3 are plotted on the left and right

axes, respectively. Temperature dependence of the intensity at q_1 is shown in the inset. (c) Schematic model of the molecular association corresponding to the peak at q_1. (d) Schematic model of the molecular association giving peak at q_2. (e) Schematic model of the molecular association corresponding to the peak at q_3.

The peaks observed in the *I vs q* plots for the tetramer correspond to monomeric, dimeric and tetrameric associations as shown in Figure 5(c-e). The ratios of $q_1/q_2 \sim 2$ and $q_1/q_3 \sim 4$ indicate that the dimeric units of the tetramer are almost in the same plane, meaning that it is much less bent than the trimer. Combined with the model associations for the dimer and trimer, the number and positions of diffuse peaks detected in our SAXS experiments can be explained on the basis of a molecular conformational odd-even dependence.
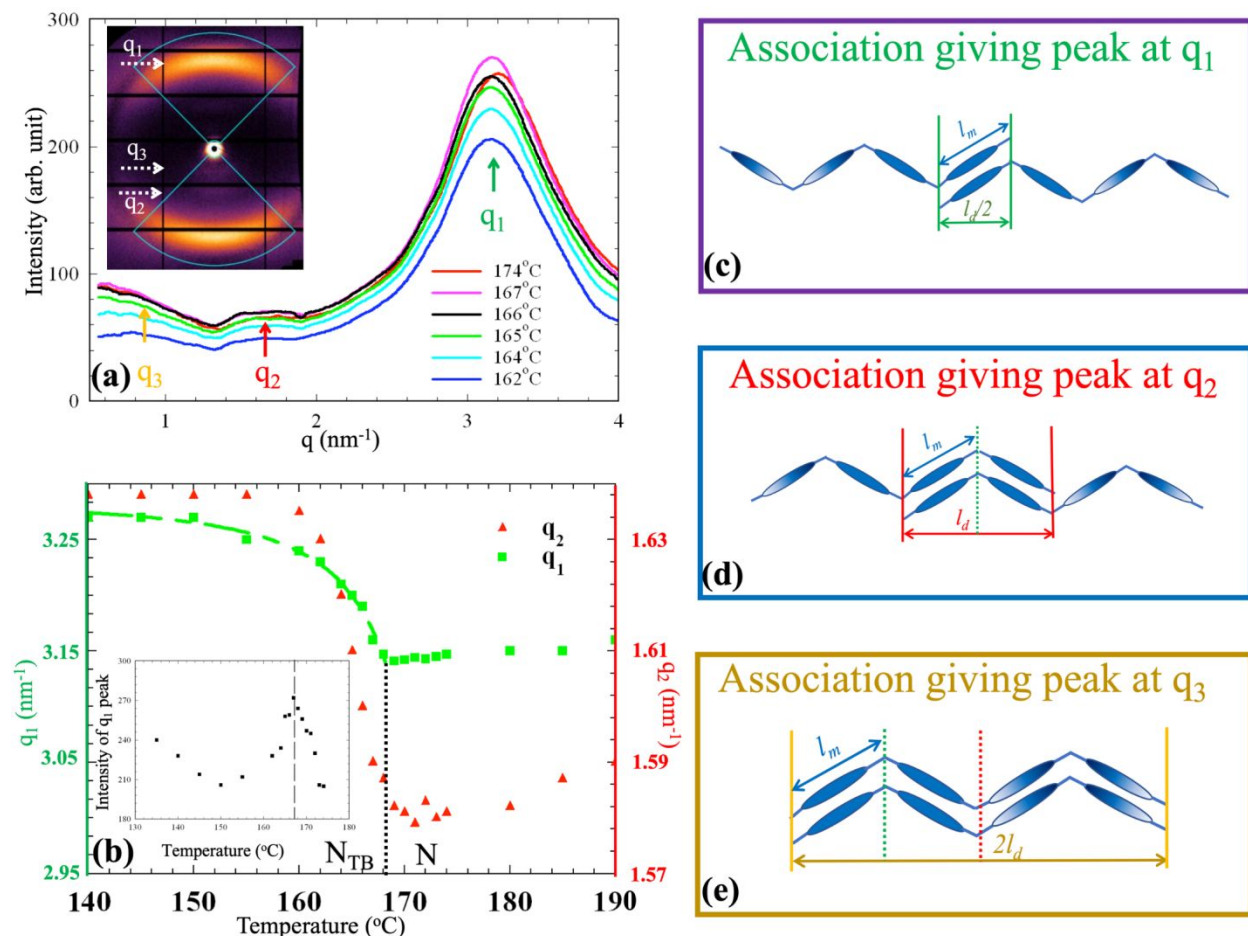

Figure 5: Summary of the SAXS results and proposed molecular association models for the tetramer. (a) Wavenumber (q) dependence of the scattered intensity for $0.5<q<4$ nm^{-1} at selected temperatures in the N and N_{TB} phases. Inset shows the 2D SAXS pattern in the nematic phase at 2^oC above the N-N_{TB} phase transition. Dark lines represent gaps in the detector array. Sectors drawn with blue lines indicate the areas over which the intensity (I) was azimuthally averaged in

order to produce the plots of I vs q (nm⁻¹) shown in the main pane. Maxima of the peaks are denoted by q_1, q_2 and q_3. (b)Temperature dependences of q_1 and q_2 are plotted on the left and right axes, respectively. Temperature dependence of the intensity at q_1 is shown in the inset. (c) Schematic model of the molecular association corresponding to the peak at q_1. (e) Schematic model of the molecular association giving peak at q_2. (d) Schematic model of the molecular association corresponding to the peak at q_3.

The variation of q_1 and q_2 with normalized temperature is shown in Figures 3-5 (b). The trends are similar for all three materials: on cooling from the isotropic phase q_1 and q_2 decrease and become almost constant before the transition to the N_{TB} phase, then they increase sharply below the transition. In the N phase the values of q_1 increase monotonously from dimer to trimer and tetramer. This is consistent with an increasing monomer-monomer bend toward higher oligomers, which reduces the average spacing between monomer units. Upon the transition to the N_{TB} phase, q_1 increases in all n=2-4 oligomers, indicating either additional increase of the bend angle, or a tilt of monomeric associations with respect to the nanoscale heliconical axis. Greater conformational bend in the N_{TB} phase should also correlate with an increase in the nanoscale pitch of the heliconical structure, as the pitch is determined by the local packing of the n-mers and higher intrinsic bend would be relieved by twist over a shorter distance. This temperature dependence is in accord with RSoX measurements for dimers of the DTC class of materials[43] and recent detailed NMR measurements of the twisting on cyanobiphenyl based dimers.[25]

Although the correlation lengths of the molecular associations were found to be continuously increasing over the entire N and N_{TB} range for all three materials (without any jump at the *N-N_{TB}* transition)[32], the temperature dependences of q_1 below the N-TB transition show an additional odd-even effect, namely a continuous change in the dimer (Figure 3(b)) and tetramer (Figure 5(b)) and a discontinuous one in the trimer (Figure 4(b)). We therefore infer a more continuous increase of the pitch wavenumber $q_0(T)$ in the even n-mers versus the odd one, where q_1 exhibits a sharper jump at the transition over a similar step in temperature. On this basis, we suggest that the pitch changes more weakly in the trimer as the N-N_{TB} transition is approached from below and has a stronger pretransitional temperature-dependence in the even n-mers. As we have already mentioned, such behavior has been reported from direct RSoXS measurements of q_0 on a homologous dimer and trimer based on a different monomeric unit. [31]

As demonstrated in the insets of Figures 3(b) – 5(b), the intensities of the q_1 peaks increase on cooling through the N phase at rates of ~4 counts/ºC for the dimer, <2 counts/ ºC for trimer and

~7 counts/$^\circ$C for tetramer. Since the intensities of the peaks at q_2 and q_3 are much smaller than for the peak at the q_1, the contribution of possible higher harmonics of q_2 and q_3 to the intensity at q_1 may be neglected. Therefore, the increase of the q_1 peak intensities observed above N-N$_{TB}$ transition may indicate a larger population of monomer-type associations between neighboring dimers. As shown in Figure 3(c), these associations lead to an increase of the apparent length of the dimers by making the structure of the associated molecules similar to a trimer, which is more linear. A more linear conformational envelope implies a larger K_{33}, which might explain the observed pretransitional increase of K_{33} in the dimer (see Figure 2(c)). Similar arguments also explain the pretransitional increase for tetramer, since the same mesogen associations lead to an increase of the effective length by three monomer units (Figure 5(c)), producing an effective length of seven units for the associated tetramers. For trimers the situation is different, as the rate of increase is smaller and because the mesogenic association still produces an odd number of mesogenic units along the contour of the associated trimers (Figure 3(d)), and therefore the degree of linearity remains the same.

At the transition to the N$_{TB}$ phase, the intensities of the q_1 peaks drop sharply (especially for the trimer). This drop is probably related to the transient disordering of the monomer-monomer association as the nanoscale heliconical molecular arrangement builds up. The observed larger drop of the intensity at q_1 in the case of the trimer can be attributed to a more discontinuous development of the heliconical structure at the N-N$_{TB}$ transition. On further cooling in the N$_{TB}$ phase, the intensity at q_1 begins to increase. The increase is notably weaker for the trimer than for the dimer or tetramer. In the case of the dimer, we expect the diffracted intensity at q_1 to increase more strongly at low temperature due to the presence of a SmX phase in this material.

Conclusions

We have experimentally investigated the temperature dependences of the birefringence and small angle x-ray scattering patterns for n=1-4 oligomers. We found that the birefringence, nematic temperature ranges, the bend elastic constants, and the number and length of positional correlations lengths of the molecular associations all show odd-even effect with respect to the number of mesogenic units in the n-mers. This effect is clearly different from previously reported and well understood odd-even effect based on the number of methylene groups in the connecting chains.

Far from the N-N$_{TB}$ transition temperature, the odd-even effect can be attributed to the overall conformation of the molecules, while near the N-N$_{TB}$ transition the effect observed in K_{33} can be understood by the behavior of the mostly populated monolayer-type associations. We also demonstrate that even in the absence of long-range electron density modulation, careful analysis of synchrotron SAXS results can provide important information about the molecular associations both in the N and N$_{TB}$ phases. This is especially significant for the studied n-mers, where repeated attempts[44] using carbon RSoXS on the pure n-mer materials failed to detect the nanoscale modulation in the N$_{TB}$ phase. Instead selenium substitution on the dimer combined with hard x-ray resonance was necessary to observe the modulation.[43] [45] Finally, we note that the observed novel odd-even effect offers an novel and facile way to tune the physical properties – such as phase range, birefringence, and the elastic constant associated with bend distortions of the optical axis – in liquid crystal oligomers by mixing odd and even n-mers in suitable ratios.

Acknowledgments

Contributions

RS, GB, ZP, MR, PG did experiments, CW and GHM synthetized materials, JG, ODL, SS, AJ, RS, GB, ZP analyzed results, AJ and SS wrote the paper.

References:

1   A. Baeyer, *Ber. Chem. Ges.*, 1877, **10**, 1286–1288.

2   R. Boese, H.-C. Weiss and D. Blaeser, *Angew. Chem. Int. Ed*, 1999, **38**, 988–992.

3   D. Vorländer, *Z Phys Chem A*, 1927, 126–449.

4   J. Rault, L. Liébert and L. Strzelecki, *B Soc Chim Fr II-Ch.*, 1975, **5**, 1175–8.

5   A. C. Griffin, N. W. Buckley, W. E. Hughes and D. L. Wertz, *Mol. Cryst. Liq. Cryst.*, 1981, **64**, 139–144.

6   C. T. Imrie and P. A. Henderson, *Chem. Soc. Rev.*, 2007, **36**, 2096–124.

7   G. R. Luckhurst, *Macromol. Symp.*, 1995, **96**, 1–26.

8   G. R. Luckhurst, *Liq. Cryst.*, 2005, **32**, 1335–1364.

9   G. Ungar, V. Percec and M. Zuber, *Macromolecules*, 1992, **25**, 75–80.

10   J. W. Emsley, G. R. Luckhurst, G. N. Shilstone and I. Sage, *Mol. Cryst. Liq. Cryst.*, 1984, **102**, 223–233.

11   J. W. Emsley, G. R. Luckhurst and G. N. Shilstone, *Mol. Phys.*, 1984, **53**, 1023–1028.

12   M. Cestari, S. Diez-Berart, D. A. Dunmur, A. Ferrarini, M. R. De La Fuente, D. J. B. Jackson, D. O. Lopez, G. R. Luckhurst, M. A. Perez-Jubindo, R. M. Richardson, J. Salud, B. A. Timimi and H. Zimmermann, *Phys. Rev. E*, 2011, **84**, 031704.

13   M. Šepelj, A. Lesac, U. Baumeister, S. Diele, H. L. Nguyen and D. W. Bruce, *J. Mater. Chem.*, 2007, **17**, 1154–1165.

14   V. Panov, M. Nagaraj, J. Vij, Y. Panarin, A. Kohlmeier, M. Tamba, R. Lewis and G. Mehl, *Phys. Rev. Lett.*, 2010, **105**, 167801.

15   A. Jákli, O. D. Lavrentovich and J. V. Selinger, *Rev. Mod. Phys.*, 2018, **90**, 045004.

16   V. Borshch, Y.-K. Kim, J. Xiang, M. Gao, A. Jakli, V. P. Panov, J. K. Vij, C. T. Imrie, M. G. Tamba, G. H. Mehl and O. D. Lavrentovich, *Nat. Commun.*, 2013, **4**, 2635-1–8.

17   D. Chen, J. H. Porada, J. B. Hooper, A. Klittnick, Y. Shen, M. R. Tuchband, E. Korblova, D. Bedrov, D. M. Walba, M. A. Glaser, J. E. Maclennan and N. A. Clark, *Proc. Natl. Acad. Sci.*, 2013, **110**, 15931–15936.

18   S. L. Abbott, B. A. Portoni and J. M. Janda, *J. Clin. Microbiol.*, 1999, **37**, 4177–4178.

19   C. Meyer, G. R. Luckhurst and I. Dozov, *Phys. Rev. Lett.*, 2013, **111**, 067801.

20   E. Gorecka, M. Salamonczyk, A. Zep, D. Pociecha, C. Welch, Z. Ahmed and G. H. Mehl, *Liq. Cryst.*, 2015, **42**, 1–7.

21   P. A. Henderson and C. T. Imrie, *Liq. Cryst.*, 2011, **38**, 1407–1414.

22   K. Adlem, M. Čopič, G. R. Luckhurst, A. Mertelj, O. Parri, R. M. Richardson, B. D. Snow, B. A. Timimi, R. P. Tuffin and D. Wilkes, *Phys. Rev. E*, 2013, **88**, 022503.

23   V. Görtz, C. Southern, N. W. Roberts, H. F. Gleeson and J. W. Goodby, *Soft Matter*, 2009, **5**, 463.

24   D. Chen, J. H. Porada, J. B. Hooper, A. Klittnick, Y. Shen, M. R. Tuchband, E. Korblova, D. Bedrov, D. M. Walba, M. A. Glaser, J. E. Maclennan and N. A. Clark, *Proc. Natl. Acad.*

Sci. U. S. A., 2013, **110**, 15931–15936.

25   J. Carvalho, C. Cruz, J. L. Figueirinhas, M. G. Tamba, A. Kohlmeier and G. H. Mehl, *J. Phys. Chem. B*, 2019, **123**, 1442–1451.

26   C. Zhu, M. R. Tuchband, A. Young, M. Shuai, A. Scarbrough, D. M. Walba, J. E. Maclennan, C. Wang, A. Hexemer and N. A. Clark, *Phys. Rev. Lett.*, 2016, **116**, 147803.

27   R. J. Mandle, *Soft Matter*, 2016, **12**, 7883–7901.

28   R. J. Mandle and J. W. Goodby, *RSC Adv.*, 2016, **6**, 34885–34893.

29   R. J. Mandle, M. P. Stevens and J. W. Goodby, *Liq. Cryst.*, 2017, **44**, 2046–2059.

30   F. F. P. Simpson, R. J. Mandle, J. N. Moore and J. W. Goodby, *J. Mater. Chem. C*, 2017, **5**, 5102–5110.

31   M. R. Tuchband, D. A. Paterson, M. Salamończyk, V. A. Norman, A. N. Scarbrough, E. Forsyth, E. Garcia, C. Wang, J. M. D. Storey, D. M. Walba, S. Sprunt, A. Jákli, C. Zhu, C. T. Imrie and N. A. Clark, *PNAS*, 2019, in print.

32   Z. Parsouzi, G. Babakhanova, M. Rajabi, R. Saha, P. Gyawali, T. Turiv, A. R. Baldwin, C. Welch, G. H. Mehl, J. T. Gleeson, A. Jakli, O. D. Lavrentovich and S. Sprunt, *Phys. Chem. Chem. Phys.*, submitted.

33   G. Cukrov, Y. M. Golestani, J. Xiang, Y. A. Nastishin, C. Welch, G. H. Mehl and O. D. Lavrentovich, *Liq. Cryst.*, 2017, **44**, 219–231.

34   N. Sebastián, M.-G. Tamba, R. Stannarius, M. R. de la Fuente, M. Salamonczyk, G. Cukrov, J. T. Gleeson, S. Sprunt, A. Jakli, C. Welch, Z. Ahmed, G. H. Mehl and A. Eremin, *Phys. Chem. Chem. Phys.*, 2016.

35   J. W. Emsley, M. Lelli, H. Joy, M. G. Tamba and G. H. Mehl, *Phys. Chem. Chem. Phys.*, 2016, **18**, 9419–9430.

36   P. G. de Gennes and J. Prost, *The Physics of Liquid Crystals*, Clarendon Press; Second Edition edition, Oxford, 1993.

37   H. Gruler, *J. Chem. Phys.*, 1974, **61**, 5408–5412.

38   W. Helfrich, *Mol. Cryst. Liq. Cryst.*, 1974, **26**, 1–5.

39   P. Sathyanarayana, M. Mathew, Q. Li, V. S. S. Sastry, B. Kundu, K. V.Le, H. Takezoe and S. Dhara, *Phys. Rev. E*, 2010, **81**, 010702(R).

40   M. Majumdar, P. P. Salamon, A. Jákli, J. T. Gleeson and S. N. Sprunt, *Phys. Rev. E*, 2011, **83**, 031701.

41   P. Tadapatri, U. S. Hiremath, C. V Yelamaggad and K. S. Krishnamurthy, *J. Phys. Chem. B*, 2010, **114**, 1745–50.

42   P. S. Salter, C. Tschierske, S. J. Elston and E. P. Raynes, *Phys. Rev. E*, 2011, **84**, 031708.

43   W. D. Stevenson, Z. Ahmed, X. B. Zeng, C. Welch, G. Ungar and G. H. Mehl, *Phys. Chem. Chem. Phys.*, 2017, **19**, 13449–13454.

44   M. Salamonczyk, *private communicaton*, 2018.

45   H. Zou, G. H. Mehl, G. Ungar, W. D. Stevenson, X. Zeng and C. Welch, *Phys. Chem. Chem. Phys.*, 2018, **20**, 25268–25274.